BeBeC-2020-D10

Virtual rotating array methods for arbitrary microphone configurations

Simon Jekosch[1], Gert Herold[1] and Ennes Sarradj[1]

[1]Technische Universität Berlin
Einsteinufer 25, 10587 Berlin, Germany

Abstract

The characterisation of rotating aeroacoustic sources using microphone array methods has been proved to be a useful tool. One technique to identify rotating sources is the virtual rotating array method. The method interpolates the pressure time data signals between the static microphone array to compensate the motion of the rotating source. One major drawback of the method is the need of ring array geometries that are centred around the rotating axis. This contribution extends the virtual rotating array method to arbitrary microphone configurations. Two different ways to interpolate the time signals between the microphone locations are compared. The first method constructs a mesh between the microphone positions using delaunay-triangulation and interpolates over the mesh faces using piecewise linear or polynomial functions. The second one is a meshless technique which is based on radial basis function interpolation. For the validation of the method, an experiment with a five-bladed fan in combination with a spiral array as well as a ring array geometry was carried out. The different interpolation algorithms are applied to the measurement data and the results are compared to the interpolation method with a ring array. The motion-compensated pressure time data is used to perform beamforming in the frequency domain and various deconvolution approaches are applied.

1 INTRODUCTION

Microphone arrays methods can be used to detect sound sources on rotating machinery. Various methods for identifying rotating noise source have been tested. These methods for processing array data are available in time domain and frequency domain. Time domain approaches using a rotating focus point have been applied for wind turbine and helicopter blades [17]. Frequency domain methods were firstly used for induct measurements [5, 10]. Those approaches solve the Green's function for a rotating acoustic source. This strategy was also adapted for free field

conditions [12]. Another method in the frequency domain to determine the location of acoustic sources is the virtual rotating array (VRA) method [8]. It compensates the motion of the source by virtually rotating the arrays microphone positions.

Axial blowing fans are widely used in many fields of application. Since the aeroacoustic design of fans is a challenging task those fans have been subject of various microphone array measurements [5, 9, 11, 20] using time domain as well as frequency domain beamforming. Measurements using the VRA method and frequency domain also rely on evenly spaced microphone placements in a ring around the center of the rotation. This contribution shows an extension of the VRA method to microphone configurations in a plane. The algorithm is also capable of interpolating pressure time data for 3D microphone arrangements.

The method is used to show differences in source localisation of a fan between a ring and a spiral array geometry.

2 METHODS

2.1 Virtual rotating array method

The motion compensation with a virtual rotating array described by Herold and Sarradj [8] tracks the angular position of the rotating source and pressure signals at the virtual microphones rotate at the same rate as the source. The signals at the virtual sensor positions are interpolated from neighbouring microphones. For a ring array with M equidistant microphones the angle α per microphone is:

$$\alpha = \frac{2\pi}{M} \tag{1}$$

and the indices of preceding and following real microphones are:

$$m_l(m,t) = \left\lfloor m + \frac{\varphi(t)}{\alpha} - 1 \right\rfloor \bmod M + 1 \tag{2}$$

$$m_\mathrm{u}(m,t) = \left\lfloor m + \frac{\varphi(t)}{\alpha} \right\rfloor \bmod M + 1 \tag{3}$$

where $\lfloor \bullet \rfloor$ denotes the floor operator and $\varphi(t)$ the azimuthal angle of the virtual rotating array. The linear interpolation weights for the microphones are calculated by

$$s_\mathrm{u}(t) = \frac{\varphi(t)}{\alpha} - \left\lfloor \frac{\varphi(t)}{\alpha} \right\rfloor \tag{4}$$

$$s_1(t) = 1 - s_\mathrm{u}(t) \tag{5}$$

and lead to the sound pressure signal at the virtual microphone positions:

$$p_{\mathrm{vr},m}(t) = s_1 p_{m_1} + s_\mathrm{u} p_{m_\mathrm{u}} \tag{6}$$

The VRA method with a ring array uses only microphone indices to determine between which microphones the interpolation has to be calculated. Since every point on the ring has exactly

2 neighbouring microphones this approach is suitable. When using arbitrary microphone geometries the neighbouring microphones cannot be deduced from the microphone indices, which makes this interpolation method insufficient. For the extension of this algorithm to 2D and 3D array geometries an interpolation process that is based on the microphone positions has to be applied. In this contribution two methods are proposed for the interpolation over unstructured microphone positions: mesh-based triangulation and radial basis function approximation.

2.2 Triangulation

For the first method a mesh needs to be constructed between all neighbouring microphones. A common way to derive such a mesh is the Delaunay triangulation [4]. The triangulation for the microphone positions x_k is constructed in such a way that all circumcircles of all triangles have empty interiors i.e. no other microphone position lies inside the circle. For this contribution all Delaunay triangulations have been calculated with the *qhull* package which is based on the quickhull algorithm by Barber et al. [1].

The interpolation between the points in the Delaunay triangulation is achieved by interpolation between neighbouring points. For a 2D Microphone geometry each point in the plane has three neighbouring points in a triangle for the interpolation. The interpolation of the sound pressure $p(x_i)$ between those three points $p(x_1), p(x_2), p(x_3)$ is achieved either by linear barycentric interpolation

$$p(x_i) = \beta_1 p(x_1) + \beta_2 p(x_2) + \beta_3 p(x_3) \tag{7}$$

with β_1, β_2 and β_3 being the normed barycentric coordinates at the point x_i or cubic spline interpolation using the Clough-Toucher algorithm [3, 7].

2.3 Radial basis functions

The meshless method for the virtual rotation uses radial basis function interpolation. A radial basis function (RBF) is an n-dimensional radially symmetric function $\Phi : \mathbb{R}^n \to \mathbb{R}$ which depends only on the Euclidean distance between the center of the RBF x_k and the point of evaluation x. The Euclidean distance is defined as $r = (\|x - x_k\|_2)$. There are various RBF's available in the literature that can be used for interpolation [2].

For the interpolation of the pressure data two different kind of basis functions are used. The first ones are multiquadric basis functions of the form $\Phi(r) = \sqrt{(r \cdot \varepsilon)^2 + 1)}$ with the scaling factor ε. The second kind are cubic basis functions $\Phi(r) = r^3$.

The pressure time signal is reconstructed at any point x by a linear combination of the RBF's centred at the known points x_k multiplied by the weight coefficients w_i:

$$p(x) = \sum_{i=0}^{M} w_i(x)\ \Phi(\|x - x_k\|_2) \tag{8}$$

and the weight coefficients are determined by solving the linear system

$$\begin{bmatrix} \Phi(\|x_0-x_0\|_2) & \Phi(\|x_1-x_0\|_2) & \cdots & \Phi(\|x_M-x_0\|_2) \\ \Phi(\|x_0-x_1\|_2) & \Phi(\|x_1-x_1\|_2) & \cdots & \Phi(\|x_M-x_1\|_2) \\ \vdots & \vdots & \ddots & \vdots \\ \Phi(\|x_0-x_M\|_2) & \Phi(\|x_1-x_M\|_2) & \cdots & \Phi(\|x_M-x_M\|_2) \end{bmatrix} \begin{bmatrix} w_1 \\ w_2 \\ \vdots \\ w_M \end{bmatrix} = \begin{bmatrix} p_1 \\ p_2 \\ \vdots \\ p_M \end{bmatrix} \tag{9}$$

with $p_0 \cdots p_M$ being the discrete pressure values at the microphone positions. This linear system can be solved iteratively and results in new time signals $p(x)$ at any virtual microphone position.

2.4 Beamforming and deconvolution

The virtual rotating array method is based on beamforming in the frequency domain and is based on the calculation of the cross spectral matrix ($\boldsymbol{C}$). It can be computed using Welch's method [18]:

$$\boldsymbol{C} = \frac{1}{K} \sum_{k=1}^{K} \boldsymbol{p}_k \boldsymbol{p}_k^H \tag{10}$$

with the number of blocks K , onto which an FFT is applied, resulting in a complex pressure vector $\boldsymbol{p}_k$ for each discrete frequency. The beamforming output (the squared sound pressures at one of the N focus points $\boldsymbol{x_s}$) in the frequency domain is calculated via

$$b(\boldsymbol{x_s}) = \boldsymbol{h}^{\mathrm{H}}(\boldsymbol{x_s})\, \boldsymbol{C}\, \boldsymbol{h}(\boldsymbol{x_s}), \quad s = 1,...,N \tag{11}$$

using the steering vector $\boldsymbol{h}$, which is chosen according to formulation III from [13]:

$$h_m = \frac{1}{r_{s,0} r_{s,m} \sum_{l=1}^{M} {r_{s,l}}^{-2}}\, e^{-jk(r_{s,m}-r_{s,0})}, \quad m = 1...M. \tag{12}$$

with the number of microphones M, $r_{s,m}$ and $r_{s,l}$ indicating the distance between the source and the microphone location and $r_{s,0}$ between the source and the array center location. This formulation has been shown theoretically to yield the correct source level [13].

Since the virtual rotating array method compensates the motion of the sources subsequent deconvolution algorithms are easily applicable. In this contribution two different deconvolution algorithms are used: CLEAN-SC [16] and covariance matrix fitting (CMF) [19].

The CLEAN-SC method starts with the conventional beamforming output. It takes the first maximum in the source map and identifies coherent parts. Than deletes these Parts from the dirty source map and finds the next remaining maximum in the remaining map. This procedure is repeated until no more significant sources are found. The CLEAN-SC result only retains the respective maximum values.

Covariance matrix fitting is inverse source localisation method which tries to model a cross spectral matrix C_{mod} with a known sound propagation matrix for monopoles from the grid of possible sources to the microphones $\boldsymbol{A}$ and the unknown sound pressure amplitudes at the grid points $\boldsymbol{D}$:

$$\boldsymbol{C}_{mod} = \boldsymbol{A}\boldsymbol{D}\boldsymbol{A}^H \tag{13}$$

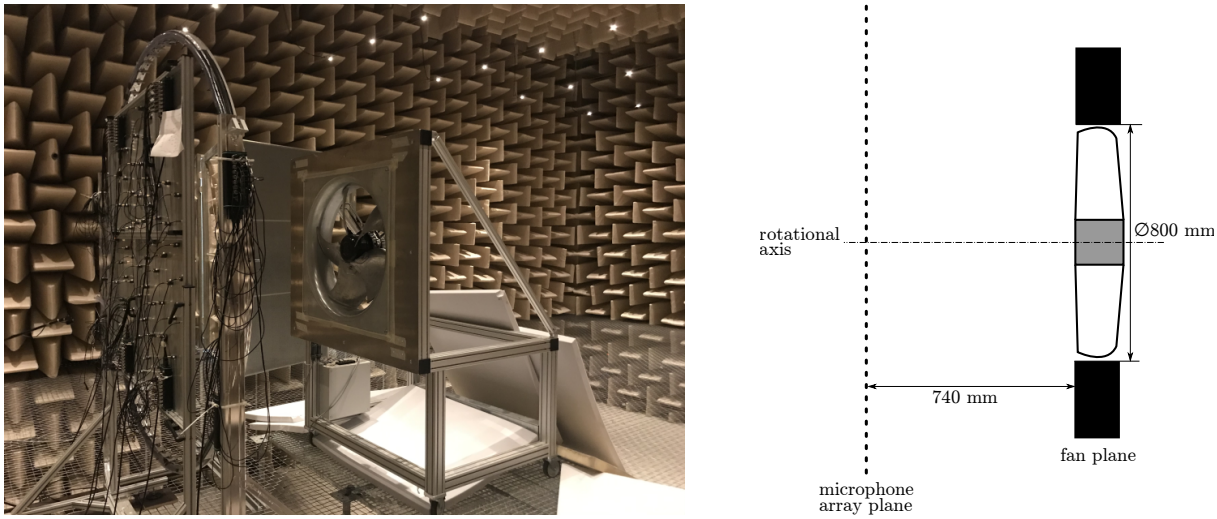

(a) Photograph of the setup (b) Side view of the setup

Figure 1: Fan measurement setup in the anechoic chamber at TU Berlin

The convex optimization problem can be written as the following function:

$$\arg\min_{\boldsymbol{D}} \|\boldsymbol{C} - \boldsymbol{A}\boldsymbol{D}\boldsymbol{A}^H\|_2 + \alpha\|\boldsymbol{D}\|_1 , \quad \alpha, \boldsymbol{D} \geq 0 \tag{14}$$

where α is an additional penalty term to enforce a sparse solution. The system can be solved using a Least Angle Regression Lasso algorithm [6].

3 APPLICATION

In order to test the different interpolation techniques acoustic measurements of a five-bladed fan has been conducted. The axial fan has a diameter of 800 mm and a rated rotational speed of 1020 revolutions per minute.

Two different array geometries were used simultaneously for the measurement of the acoustic pressure data. The first one been a sunflower spiral with 63 microphones. The parameters of the sunflower spiral are used according to [14] with the spiral parameters H = 1.0 and V = 5.0. The array aperture of the array is $d_{spiral} = 1.5\,\mathrm{m}$. The spiral array geometry is shown in Figure 2. The second array was a ring array which consisted of 64 microphones, arranged evenly with a radius of $d_{ring} = 2.09\,\mathrm{m}$. The type of microphones used for both arrays are GRAS 40PL-1 Short CCP. The distance between the array center and the fan was 0.74 m. In addition to the sound pressures, the rotational speed of the fan was tracked using a laser trigger. The trigger-per-revolution signal was synchronised to the pressure measurement to take into account small variations in the rotational speed of the fan. Measurement time was 40s with a sampling frequency of 51200 Hz. The beamforming output was calculated using conventional beamforming in the frequency domain as well as CLEAN-SC and CMF deconvolution. Diagonal removal of the cross spectral matrix was applied to reduce noise. The measurement was conducted anechoic chamber at TU Berlin. Figure 1 shows a Photograph of the experimental setup as well as a side view. The array measurement and data processing parameters are summarised in Table 1.

Table 1: Data acquisition and processing parameters.

Number of microphones	63/64	Focus grid distance	0.74
Spiral array aperture	1.5 m	Focus grid resolution	0.01 m
Ring array diameter	2.09 m	CMF iterations	500
Sampling rate	51.2 kHz	CMF α	10^{-12}
FFT block size	1024	CLEAN-SC iterations	500
FFT window/overlap	von Hann / 50 %	CLEAN-SC damping	0.6
Focus grid area	0.50 m $\times$ 0.50 m		

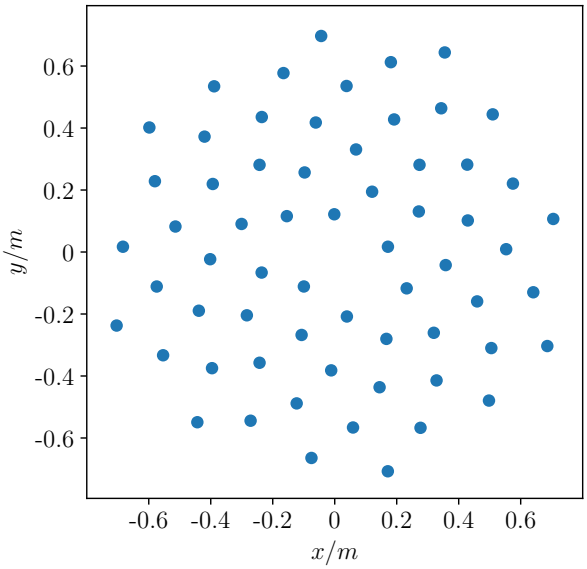

Figure 2: Spiral array geometry.

4 RESULTS

The Figures 3 to 7 show the source distribution in terms of the sound pressure level for three different center octave bands that are calculated with conventional beamforming. The maximal displayed dynamic range of the source strength is set to 15 dB.

The source map obtained with the ring array clearly differs from the spiral array results. At the octave band around 2.5 kHz the dynamic range is significantly lower for the ring array. The source maxima are at the tip of the five blades are at almost at the same positions for both arrays. For the 5 and 10 kHz octave band the ring array results tend to show high source levels at the center of the focus area. Results with the spiral array do not show this effect for 5 kHz and less distinct at 10 kHz. At 5 kHz the ring array results show reveal the source distribution along the trailing edge, while the spiral array only shows the sources at the tip of the blade. The differences between the interpolation algorithms of the time data are only visible in varying side lobes. The source positions at the tip of the blade are the same for all four algorithms. This seems plausible since the annular gap between the blade tips and the casing is an important parameter for noise generation.

The source mapped obtained with CLEAN-SC and CMF deconvolution are shown in the Fig-

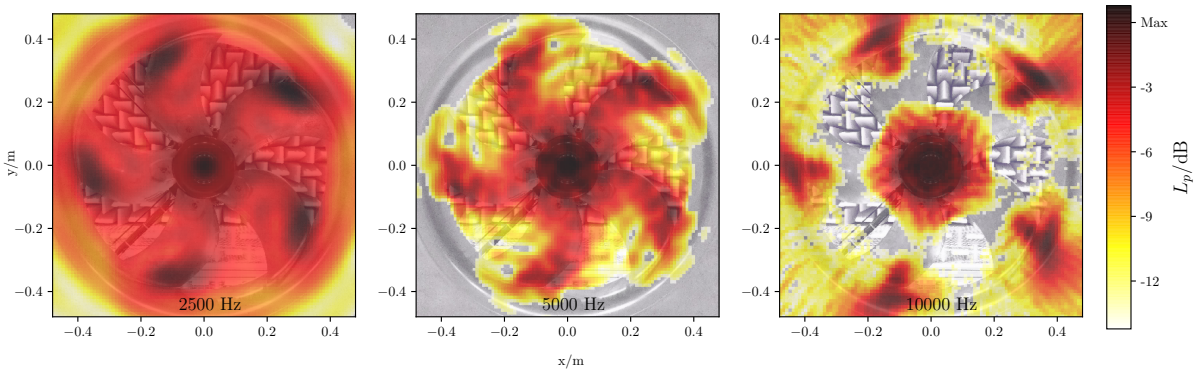

Figure 3: Octave band source maps for 2.5, 5 and 10 kHz obtained with the ring array and linear interpolation between the microphones using conventional beamforming.

ures 8 to 17. The dynamic range of the maps is increased to 30 dB. The CLEAN-SC source maps generated from the ring array also show sources in the center of the map. This effect gets stronger for higher frequencies and is mainly caused by the conventional beamforming result. Since the loudest sources are at the center the CLEAN-SC algorithms starts at those positions. For the spiral array this effect does not occur. The sources at the trailing edge is visible at 2.5 kHz. The distribution of the sources is more plausible for the interpolation with the Delauney triangulation as it follows the shape of the blade. At higher frequencies the sources at the tip are at the correct region. The CMF deconvolution results show a very accurate line of the trailing edge with the ring array. Also the sources at the center are weaker than with the CLEAN-SC algorithm. The CMF spiral array source maps are very similar to CLEAN-SC results. This comparison mainly shows that the deconvolution results for both methods are still dependent from the microphone array geometry.

For quantitative comparison, the spectra is computed by integrating the sound pressure over leading and trailing edge, the full blade and the whole focus area. Figure 18 shows the 1/3 octave spectra obtained with CLEAN-SC deconvolution. The total energy in the focus area is almost identical for all four interpolation methods. Except for frequencies above 12 kHz and below 1.6 kHz the energy in the map is dominated by the sources at the blades. The sound from the blade is mainly radiated from the tip region of the training edge. Leading edge noise is at least 10 dB lower is most cases. Only for linear interpolation at low frequencies the leading edge noise is in the same sound level region as the trailing edge. This might be due to a low spatial resolution of the beamforming output at these frequencies.

5 CONCLUSION

An extension to the original virtual rotating array method has been proposed to overcome the limitation of ring arrays. Four different methods have been derived and tested with array data from a fan measurement. Delaunay triangulation in combination with barycentric and cubic spline interpolation as well as cubic and multiquadric radial basis function interpolation was used for pressure time data interpolation.

The beamforming and deconvolution result have been compared with the original VRA method using a ring array. All methods are able to reconstruct the sound sources in a satis-

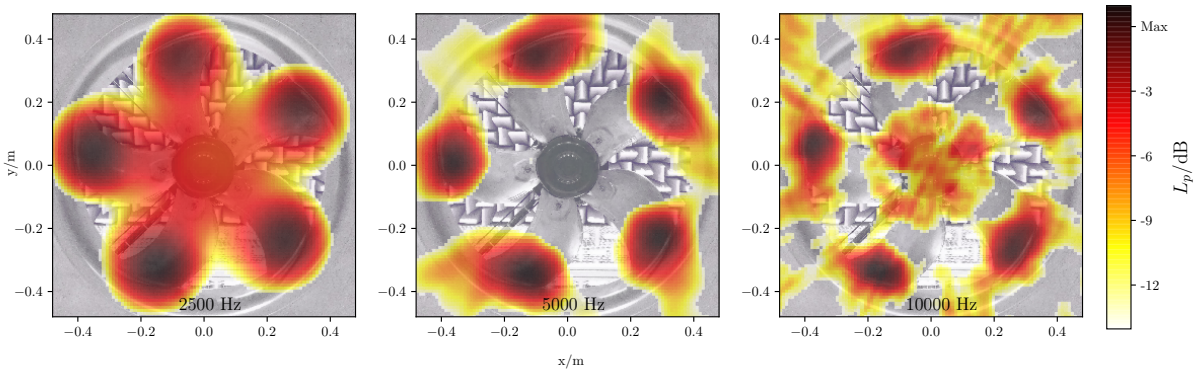

Figure 4: Octave band source maps for 2.5, 5 and 10 kHz obtained with the spiral array and linear interpolation between the microphones using conventional beamforming.

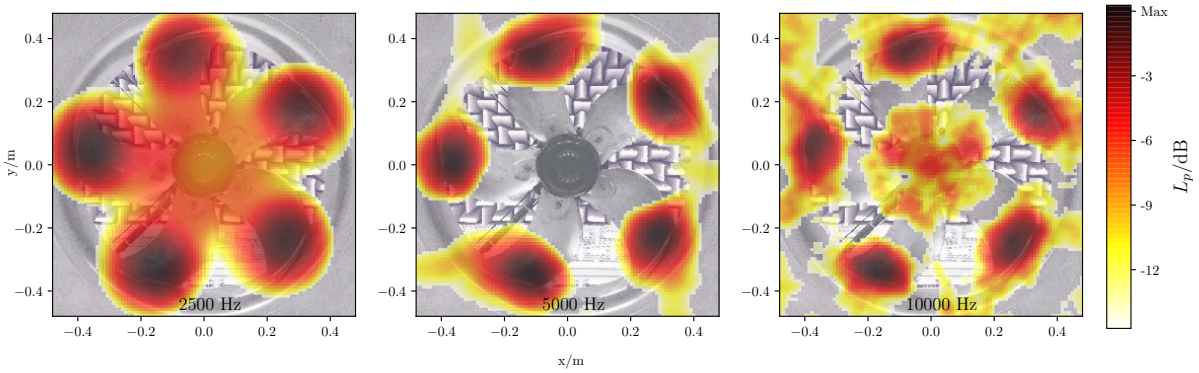

Figure 5: Octave band source maps for 2.5, 5 and 10 kHz obtained with the spiral array and Clough-Toucher spline interpolation between the microphones using conventional beamforming.

fying way. In comparison to the ring array, the tendency to indicate sources at the focus plane center is reduced. The developed method is part of the recent version of the open-source software Acoular [15].

References

[1] C. B. Barber, D. P. Dobkin, and H. Huhdanpaa. "The Quickhull Algorithm for Convex Hulls." *ACM Transactions on Mathematical Software*, 22(4), 469–483, 1996. doi:10.1145/235815.235821.

[2] M. D. Buhmann. *Radial basis functions: theory and implementations*, volume 12. Cambridge university press, 2003.

[3] R. Clough and J. Tocher. "Finite Element Stiffness Matrices for Analysis of Plates in Bending.", 1965.

[4] B. Delaunay. "Sur la sphère vide." *Classe des sciences mathematiques et na*, 6, 793–800, 1934.

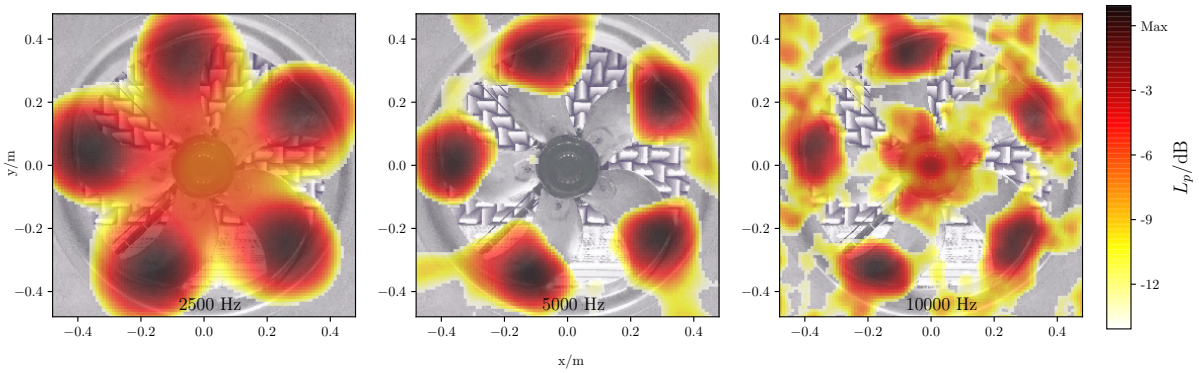

Figure 6: Octave band source maps for 2.5, 5 and 10 kHz obtained with the spiral array and cubic radial basis function interpolation between the microphones using conventional beamforming.

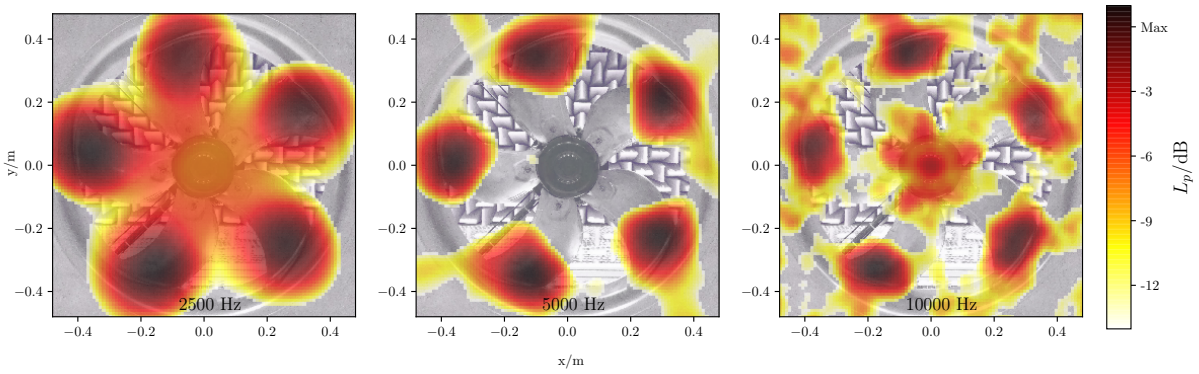

Figure 7: Octave band source maps for 2.5, 5 and 10 kHz obtained with the spiral array and multiquadric radial basis function interpolation between the microphones using conventional beamforming.

[5] R. P. Dougherty and B. Walker. "Virtual rotating microphone imaging of broadband fan noise." *15th AIAA/CEAS Aeroacoustics Conference*, 2009.

[6] B. Efron and T. Hastie. "Least angle regression." *The Annals of statistics*, 32(2), 407–499, 2004. doi:10.1214/009053604000000067.

[7] G. Farin. "A modified clough-tocher interpolant." *Computer Aided Geometric Design*, 2(1), 19 – 27, 1985. doi:https://doi.org/10.1016/0167-8396(85)90003-2.

[8] G. Herold and E. Sarradj. "Microphone array method for the characterization of rotating sound sources in axial fans." *Noise Control Engineering Journal*, 63(6), 546–551, 2015.

[9] G. Herold, F. Zenger, and E. Sarradj. "Influence of blade skew on axial fan component noise." *International Journal of Aeroacoustics*, 16(4-5), 418–430, 2017. doi:10.1177/1475472X17718740.

[10] C. Lowis and P. Joseph. "Determining the strength of rotating broadband sources in ducts

by inverse methods." *Journal of Sound and Vibration*, 295(3), 614 – 632, 2006. doi: https://doi.org/10.1016/j.jsv.2006.01.031.

[11] O. Minck, N. Binder, O. Cherrier, L. Lamotte, and V. Budinger. "Fan noise analysis using a microphone array." *Fan 2012 - International Conference on Fan Noise*, (April), 18–20, 2012.

[12] W. Pannert and C. Maier. "Rotating beamforming - Motion-compensation in the frequency domain and application of high-resolution beamforming algorithms." *Journal of Sound and Vibration*, 333(7), 1899–1912, 2014. doi:10.1016/j.jsv.2013.11.031.

[13] E. Sarradj. "Three-dimensional acoustic source mapping with different beamforming steering vector formulations." *Advances in Acoustics and Vibration*, 2012. doi: 10.1155/2012/292695.

[14] E. Sarradj. "A Generic Approach To Synthesize Optimal Array Microphone Arrangements." *Proceedings of the 6th Berlin Beamforming Conference*, pages 1–12, 2016.

[15] E. Sarradj and G. Herold. "A Python framework for microphone array data processing." *Applied Acoustics*, 116, 50–58, 2017. doi:10.1016/j.apacoust.2016.09.015.

[16] P. Sijtsma. "CLEAN based on spatial source coherence." *International Journal of Aeroacoustics*, 6, 357–374, 2007. doi:10.1260/147547207783359459.

[17] P. Sijtsma, S. Oerlemans, and H. Holthusen. "Location of rotating sources by phased array measurements." *7th AIAA/CEAS Aeroacoustics Conference and Exhibit*, 2001. doi: 10.2514/6.2001-2167.

[18] P. D. Welch. "The Use of Fast Fourier Transform for the Estimation of Power Spectra: A Method Based on Time Averaging Over Short, Modified Periodograms." *IEEE Transactions on Audio and Electroacoustics*, 15(2), 70–73, 1967. doi:10.1109/TAU.1967.1161901.

[19] T. Yardibi, J. Li, P. Stoica, and L. N. Cattafesta. "Sparsity constrained deconvolution approaches for acoustic source mapping." *The Journal of the Acoustical Society of America*, 123(5), 2631–2642, 2008. doi:10.1121/1.2896754.

[20] F. J. Zenger, G. Herold, S. Becker, and E. Sarradj. "Sound source localization on an axial fan at different operating points." *Experiments in Fluids*, 57(8), 1–10, 2016. doi: 10.1007/s00348-016-2223-8.

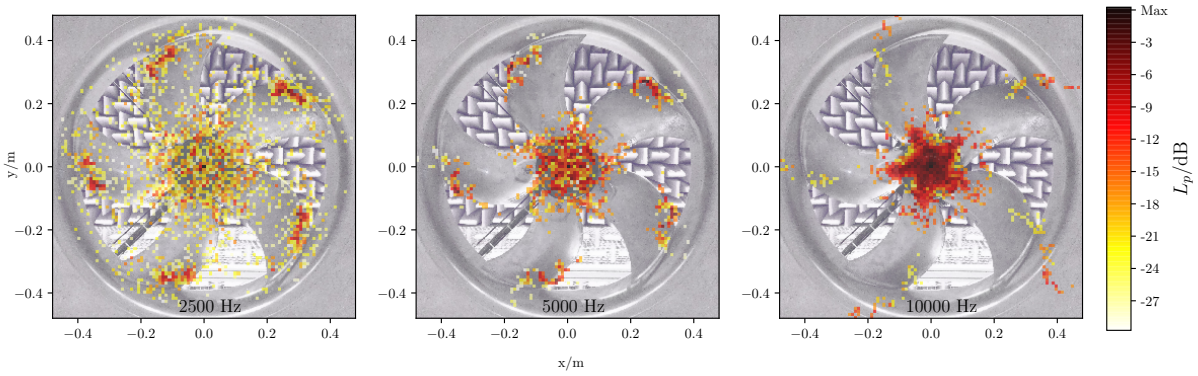

Figure 8: Octave band source maps for 2.5, 5 and 10 kHz obtained with the ring array and linear interpolation between the microphones using CLEAN-SC deconvolution.

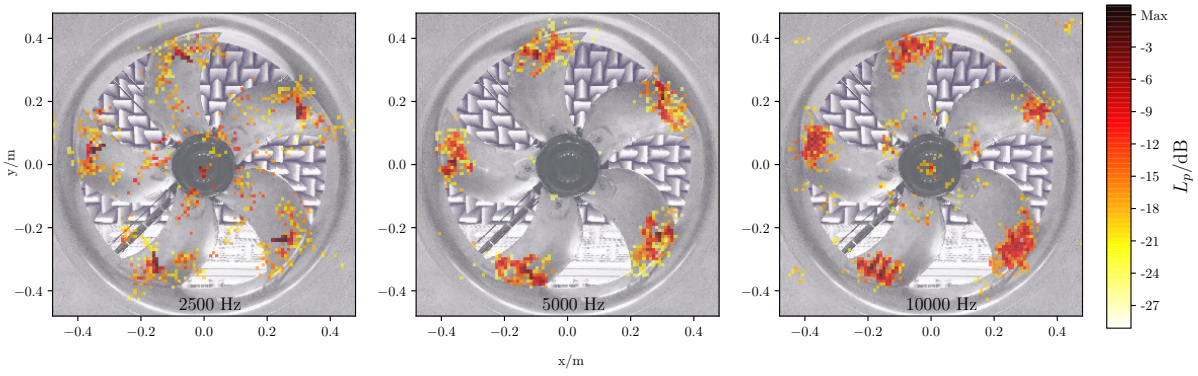

Figure 9: Octave band source maps for 2.5, 5 and 10 kHz obtained with the spiral array and linear interpolation between the microphones using CLEAN-SC deconvolution.

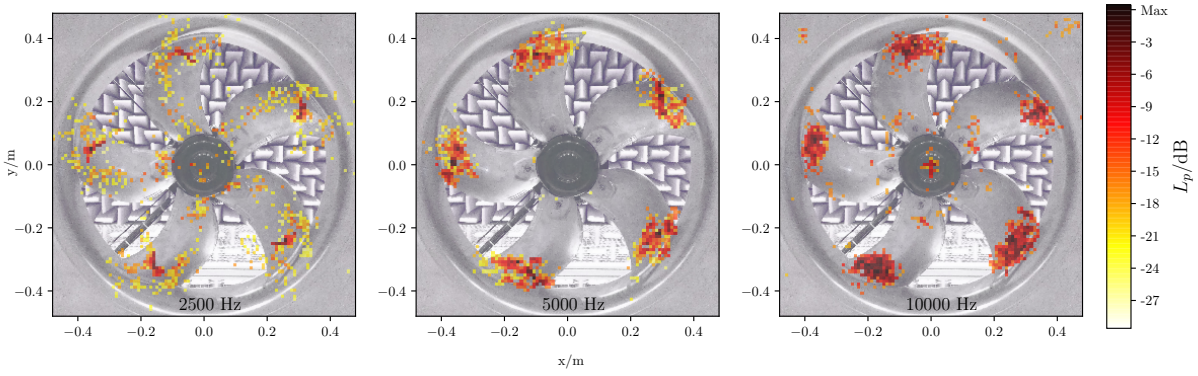

Figure 10: Octave band source maps for 2.5, 5 and 10 kHz obtained with the spiral array and Clough-Toucher spline interpolation between the microphones using CLEAN-SC deconvolution.

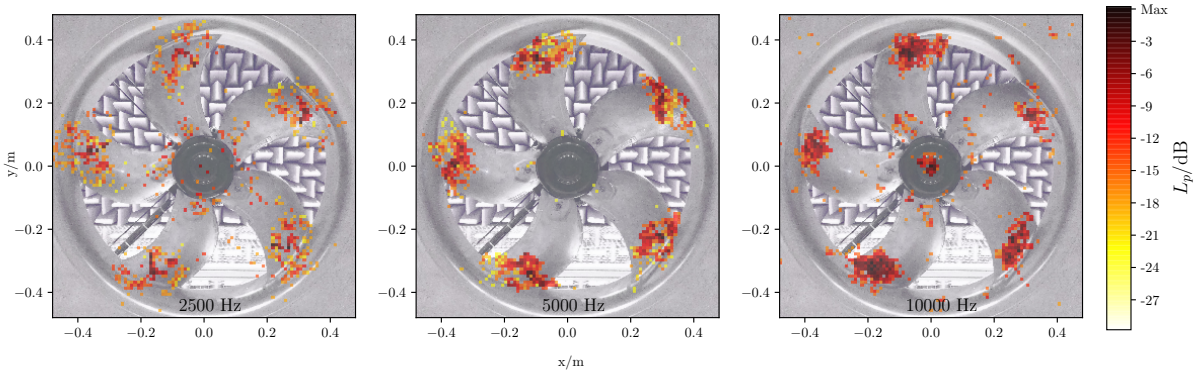

Figure 11: Octave band source maps for 2.5, 5 and 10 kHz obtained with the spiral array and cubic radial basis function interpolation between the microphones using CLEAN-SC deconvolution.

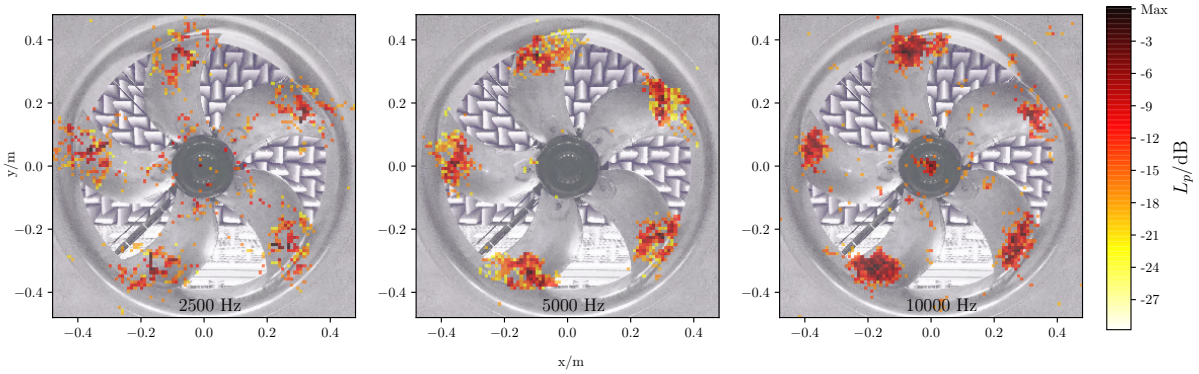

Figure 12: Octave band source maps for 2.5, 5 and 10 kHz obtained with the spiral array and multiquadric radial basis function interpolation between the microphones using CLEAN-SC deconvolution.

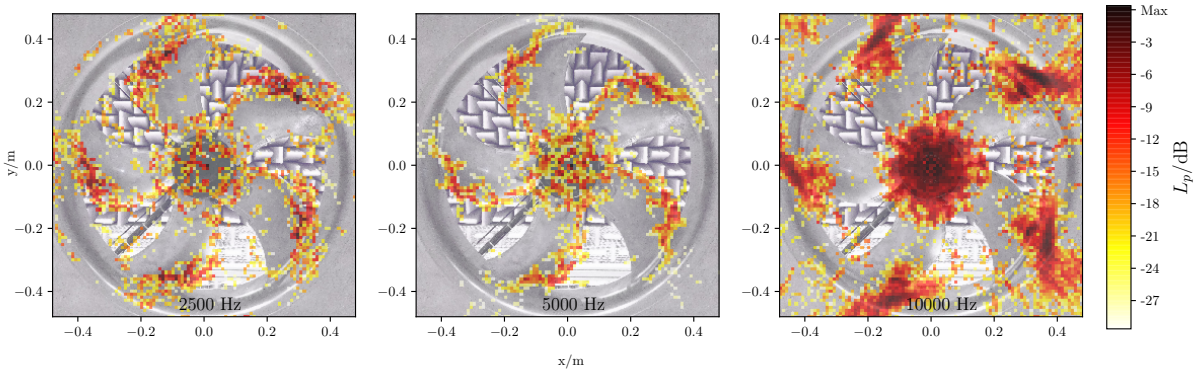

Figure 13: Octave band source maps for 2.5, 5 and 10 kHz obtained with the ring array and linear interpolation between the microphones using CMF deconvolution.

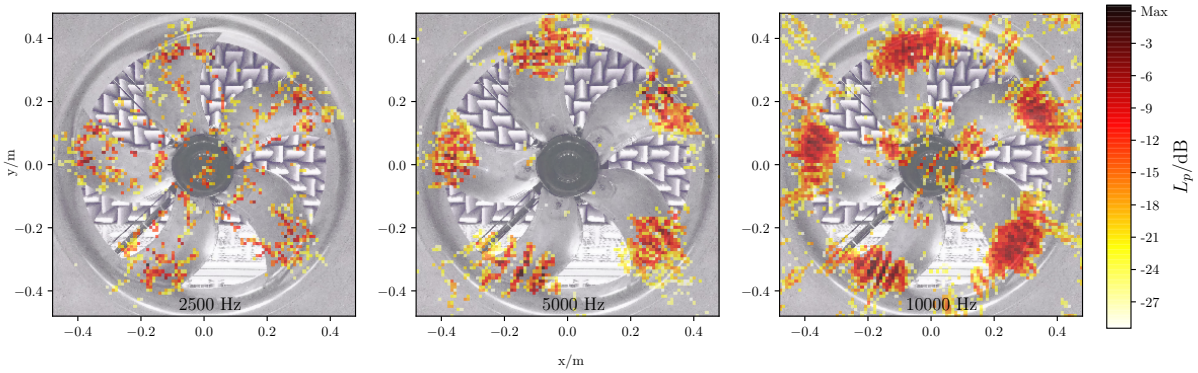

Figure 14: Octave band source maps for 2.5, 5 and 10 kHz obtained with the spiral array and linear interpolation between the microphones using CMF deconvolution.

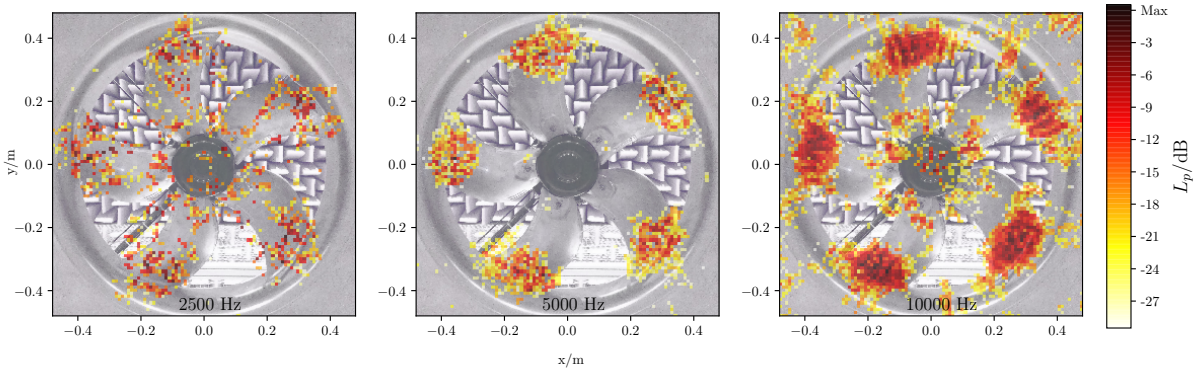

Figure 15: Octave band source maps for 2.5, 5 and 10 kHz obtained with the spiral array and Clough-Toucher spline interpolation between the microphones using CMF deconvolution.

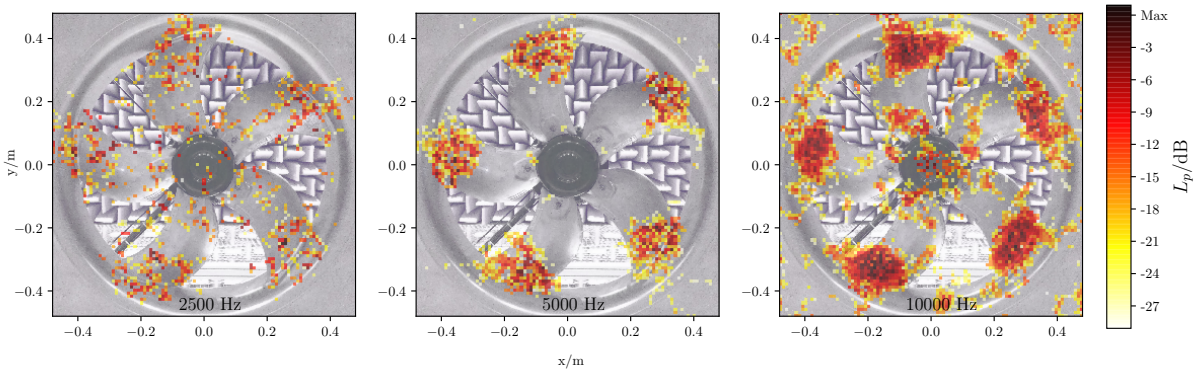

Figure 16: Octave band source maps for 2.5, 5 and 10 kHz obtained with the spiral array and cubic radial basis function interpolation between the microphones using CMF deconvolution.

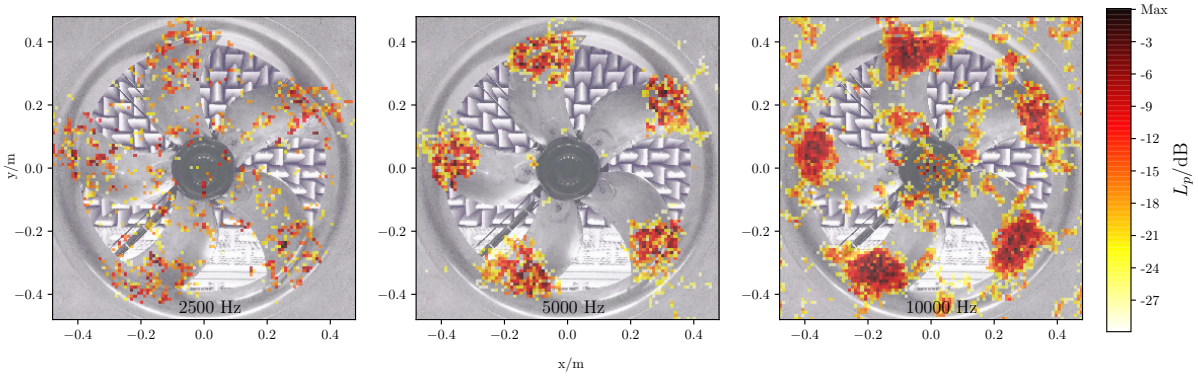

Figure 17: Octave band source maps for 2.5, 5 and 10 kHz obtained with the spiral array and multiquadric radial basis function interpolation between the microphones using CMF deconvolution.

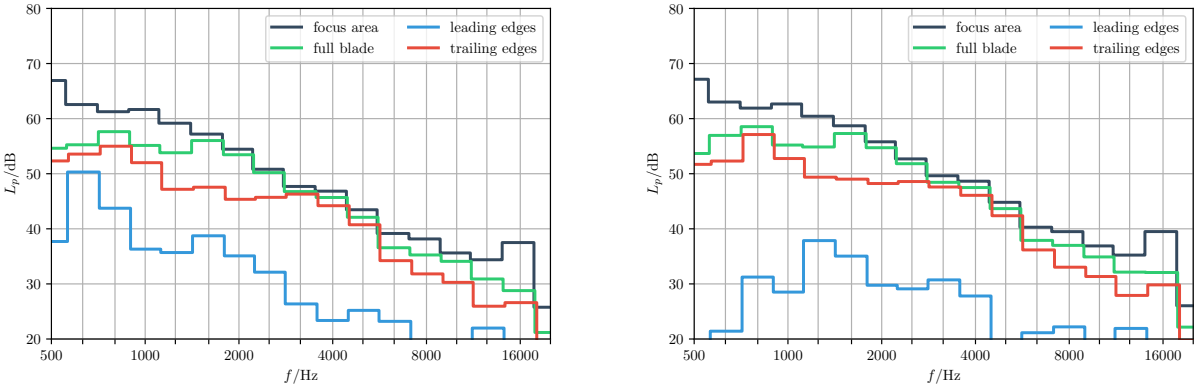

(a) Linear interpolation

(b) Spline interpolation

(c) Cubic RBF interpolation

(d) Multiquadric RBF interpolation

Figure 18: 1/3 octave band spectra for the full blade (green), leading edges (blue), trailing edges (red) and the whole focus area (black) obtained with the spiral array and using CLEAN-SC deconvolution for the different interpolation methods.